

Star Formation in Close Pairs Selected from the Sloan Digital Sky Survey

B. Nikolic* H. Cullen† P. Alexander

Astrophysics Group, Cavendish Lab., Cambridge CB3 0HE

2004/03/14

ABSTRACT

The effect of galaxy interactions on star formation has been investigated using Data Release 1 of the Sloan Digital Sky Survey (SDSS). Both the imaging and spectroscopy data products have been used to construct a catalogue of nearest companions to a volume limited ($0.03 < z < 0.1$) sample of galaxies drawn from the main galaxy sample of SDSS. Of the 13973 galaxies in the volume limited sample, we have identified 12492 systems with companions at projected separations less than 300 kpc. Star-formation rates for the volume-limited sample have been calculated from extinction and aperture corrected $H\alpha$ luminosities and, where available, *IRAS* data. Specific star formation rates were calculated by estimating galaxy masses from z -band luminosities, and r -band concentration indices were used as an indicator of morphological class. The mean specific star-formation rate is found to be strongly enhanced for projected separations of less than 30 kpc. For late-type galaxies the correlation extends out to projected separations of 300 kpc and is most pronounced in actively star-forming systems. The specific star-formation rate is observed to decrease with increasing recessional velocity difference, but the magnitude of this effect is small compared to that associated with the projected separation. We also observe a tight relationship between the concentration index and pair separation; the mean concentration index is largest for pairs with separations of approximately 75 kpc and declines rapidly for separations smaller than this. This is interpreted as being due to the presence of tidally-triggered nuclear starbursts in close pairs. Further, we find no dependence of star formation enhancement on the morphological type or mass of the companion galaxy.

Key words: galaxies: evolution – galaxies: statistics – surveys

1 INTRODUCTION

It is well established, both observationally and theoretically, that galaxies do not evolve in isolation from one another but that their present day structure is the result of sequential mergers and encounters of galaxies and proto-galaxies. For example, Toomre & Toomre (1972) used numerical simulations to show that many of the features of peculiar galaxies can be explained by recent galaxy-galaxy interactions and mergers. Indeed, in the currently widely favoured hierarchical models of galaxy formation, all of the galaxies at the present epoch are the results of mergers and accretion (e.g., Cole et al. 2000).

The problem of predicting the outcomes of galaxy encounters is difficult. Much progress has been made using numerical simulations (e.g., Mihos & Hernquist 1996), following the pioneering work of Toomre & Toomre (1972), but several outstanding problems remain. The fate of the inter-stellar medium (ISM) and even-

tual conversion to new stars is particularly difficult to follow due to the finite resolution of simulations and the complicated physics of the ISM. In this paper we investigate one aspect of this problem, the effect of tidal interaction on the star formation rate of galaxies, using data from the Sloan Digital Sky Survey (SDSS; York et al. 2000).

The connection between star formation and galaxy interactions has been suspected ever since the first large surveys, biased towards star forming systems were conducted: first in the ultraviolet continuum, then in emission lines and the far infrared. The far infrared survey by the Infrared Astronomical Satellite (*IRAS*), in particular, found a population of star forming systems in the nearby universe with $L_{\text{FIR}} > 1 \times 10^{11} L_{\odot}$, corresponding to an inferred star formation rate greater than $22 M_{\odot} \text{ year}^{-1}$. These star-forming galaxies exhibit, on average, more peculiar morphologies and are more likely to be mergers. Furthermore, these observational indications of interaction/merger become more common and pronounced in systems with higher star-formation rates. The most luminous of the *IRAS* sources, i.e., those with $L_{\text{FIR}} \geq 3 \times 10^{12} L_{\odot}$, be-

* Supported by a PPARC Studentship

† Supported by a PPARC Studentship

ing universally classified as strong interactions or mergers (Sanders & Mirabel 1996).

A number of existing studies have used samples of interacting galaxies to examine statistically the causal relationship between galaxy interactions and star formation. For example, Larson & Tinsley (1978) found a much higher dispersion in the $U - B$ versus $B - V$ colour-colour plot for galaxies selected from Arp's atlas (1966) as compared to a control sample, indicating an enhanced star formation rate within the last $\sim 10^8$ years. Kennicutt et al. (1987) used $H\alpha$ line and far infrared observations to examine the influence of interactions on the global star formation of a complete sample of close pairs, and a sample of Arp systems. They found a higher than average star formation rate in interacting systems, but also found that a large fraction of galaxies in close pairs exhibit normal star formation rates. Similarly, Bushouse et al. (1988) examined the far infrared emission in a sample of strongly interacting galaxy pairs, finding enhanced emission in some, but not all systems. Bergvall et al. (2003) have looked at star formation in a sample of 59 interacting and merging systems, and 38 isolated galaxies, using spectroscopic and photometric observations in the optical/near-infrared. In contrast to other results, they find that the global UBV colours do not support significant enhancement of the star-formation rate in interacting/merging galaxies.

Defining samples of interacting or merging galaxies to investigate the effects of interaction on star formation is not straightforward. One technique, based on the work of Toomre & Toomre (1972), is to select galaxies with peculiar morphologies, especially those showing tidal tails or galactic bridges. Such systems are often drawn from Arp's Atlas of Peculiar Galaxies (1966). This technique has been used by a number of authors, including, Larson & Tinsley (1978) and Kennicutt et al. (1987). The drawback, as illustrated by Toomre & Toomre (1972) themselves, is that the degree of morphological disturbance is sensitive to the orbital parameters of the interaction, and so can not be relied upon to trace all interactions. Additionally, the features characteristic of interaction are often of low surface brightness, requiring deep imaging for detection, and must be identified by visual inspection.

When the interacting systems are separated by distances comparable to, or larger than, their optical extents, it is relatively easy to resolve the galaxies in imaging data and, based on their projected separation, identify them as a physical pair. If spectral data are available, the velocity separation can also be used. Using this technique, survey data can be analysed for close pairs yielding large samples of interacting galaxies, albeit usually missing the galaxies in the later stages of interaction and merger.

Large area redshift surveys have enabled studies of large samples of interacting galaxies. For example, Barton et al. (2000) have analysed optical spectra from a sample of 502 galaxies in close pairs and N-tuples from the CfA2 redshift survey finding the equivalent widths of $H\alpha$ anti-correlate strongly with pair spatial and velocity separation. Similarly, Lambas et al. (2003) examined 1853 pairs in the 100k public release of the 2dF galaxy survey and find star formation in galaxy pairs to be significantly enhanced over that of isolated galaxies for separations less than 36 kpc and velocity differences less than 100 km s^{-1} .

In this paper we follow a similar approach and use the SDSS to define a large sample of 12861 galaxies with identified companions. Our aim is to establish the relative importance of galaxy interactions in determining star formation.

A number of studies have established a link between density of environment and star-formation rate, for example using the SDSS (Gómez et al. 2003), 2dF (Lewis et al. 2002), and Las Cam-

panas Redshift Survey (Hashimoto et al. 1998). In all three studies a correlation is found between density of environment and star-formation rate in the sense that ongoing star formation is suppressed in the denser environments. Gómez et al. (2003) and Hashimoto et al. (1998) have attempted to decouple this effect from the density-morphology (Dressler 1980) or radius morphology relations (Whitmore et al. 1993) finding that the density/star-formation rate relationship exists independent of the density-morphology relationship.

The structure of this paper is as follows: In Section 2 we discuss the compilation of a volume- and luminosity-limited sample drawn from the SDSS, the method used to define galaxy pairs together with details of various physical parameters calculated for each system. In Section 3 we present our results and in Section 4 we discuss these results in the context of earlier work and consider the implications for our understanding of interaction-triggered star formation.

2 THE DATA

2.1 Sloan Digital Sky Survey

The Sloan Digital Sky Survey (SDSS) is an imaging survey in five broad photometric bands (u , g , r , i , and z , defined in Fukugita et al. 1996) with medium-resolution ($R \approx 1800\text{--}2100$) spectroscopic follow up of approximately one million targets. When complete, it will cover most of the Northern Galactic Hemisphere. The sample used in this work is based on Data Release 1 (DR1) which covers 1360 deg^2 of the sky; however, we use the improved spectroscopic data for each object from Data Release 2 (DR2).

The Main Galaxy Sample (MGS, Strauss et al. 2002) was selected from the SDSS imaging data as a galaxy sample for spectroscopic observations. Objects were identified as galaxies in the SDSS imaging data if their r -band magnitude measured using the best-fitting galaxy light curve was at least 0.3 magnitudes brighter than the magnitude measured using the point spread function model. All such galaxies with r -band Petrosian magnitudes brighter than 17.77 were selected for spectroscopic follow up and were observed, as far as possible, given the fibre-placement constraints and the finite number of fibres on any one plate. The resulting completeness is 93%. Of the 7% of galaxies that are missing, 6% are galaxies which could not be observed due to the minimum fibre separation constraint.

The MGS was used to construct (Section 2.2) a volume limited sub-sample. Each member of this sub-sample was then paired with its nearest galaxy (Section 2.4) and its star formation rate estimated using two methods (Section 2.3).

2.2 Primary Catalogue

Our primary catalogue is a complete, volume- and luminosity-limited, sub-sample of the MGS. It was derived from the MGS using a procedure analogous to that used by Gómez et al. (2003). The volume of the sample was defined by the redshift constraint $0.03 < z < 0.1$, where the lower limit was used to avoid subsequent large aperture corrections when estimating star-formation rates from $H\alpha$ measurements (Section 2.3.1). The upper redshift limit allows us to construct a complete sample by retaining only galaxies with r -band absolute magnitudes $M_r < -20.45$.

Two further criteria were needed to remove a small number of

spurious entries. The first was the elimination of galaxies with redshift confidence less than 0.7. This relatively relaxed constraint removes most of the galaxies with poorly determined redshifts while introducing only a very small bias towards active emission line systems. Secondly, entries in the SDSS with Petrosian z -band magnitudes fainter than 22.83, i.e., below the detection limit (Table 21 in Stoughton et al. 2002), were excluded. Since galaxies in the main sample have $r < 17.77$, entries with $z > 22.83$ have extreme colours and are almost certainly spurious detections.

For the purposes of this study, we wish to remove systems in which an AGN provides the dominant contribution to the ionising radiation (in these cases an accurate estimate of the star-formation rate is not possible using the methods we employ). Following Veilleux & Osterbrock (1987), AGN were identified by their positions on the $[\text{N II}]/\text{H}\alpha$ vs $[\text{O III}]/\text{H}\beta$ and, in a few cases, $[\text{O I}]/\text{H}\alpha$ vs $[\text{O III}]/\text{H}\beta$ planes. We required the signal to noise ratio for the line fluxes to exceed 2 before taking them into consideration. Approximately 38% of galaxies from the volume limited sample were identified as having an AGN. Of these 64% are early- or mixed-type galaxies. A further 295 objects which were not classified spectroscopically as AGN but exhibited very broad $\text{H}\alpha$ lines with $\sigma > 570 \text{ km s}^{-1}$, were also excluded.

2.3 Star Formation Rate Estimators

Kennicutt (1998) reviews a number of widely used estimates for galaxy star-formation rate (SFR), including $\text{H}\alpha$ and $[\text{O II}]$ emission lines, together with ultraviolet, far-infrared (FIR) and radio continuum emissions. Two of these indicators with very different properties were used in this work: the $\text{H}\alpha$ line and the FIR continuum emission.

2.3.1 The $\text{H}\alpha$ line

Star formation rates, ψ , for all the galaxies in the primary catalogue were estimated from $\text{H}\alpha$ luminosities, $L_{\text{H}\alpha}$, using the relation presented in Kennicutt (1998):

$$\psi (\text{M}_{\odot} \text{ yr}^{-1}) = \frac{L_{\text{H}\alpha}}{1.27 \times 10^{34} \text{ W}}. \quad (1)$$

This relation is valid in the case of optically thin recombination, and when the star formation obeys the Salpeter (1955) initial mass function.

$\text{H}\alpha$ fluxes were calculated from line parameters measured by the SDSS spectroscopic data processing pipeline, outlined in Stoughton et al. (2002). As discussed above, while our sample is drawn from DR1, we used the DR2 spectroscopy data-products which are better calibrated and more robust. The pipeline uses a number of absorption and emission lines, and broader features, to determine redshifts from spectra. Therefore, the $\text{H}\alpha$ line need not be prominent to be measured and, indeed, in the majority of objects in our volume limited sample it is measured below the noise level or in absorption.

Corrections for dust obscuration, stellar line absorption and the $3''$ aperture were applied following the prescription presented in Hopkins et al. (2003). Both the $\text{H}\alpha$ and $\text{H}\beta$ lines were corrected for stellar absorption. The equivalent width corrections applied were 1.3 \AA and 1.65 \AA respectively. As discussed in Hopkins et al. (2003), these values are lower than the true stellar absorption because SDSS spectra resolve the absorption profile. Dust absorption correction was calculated from the observed $\text{H}\alpha/\text{H}\beta$ ratio, assuming an intrinsic ratio of 2.86 and the extinction curve presented in

Cardelli et al. (1989). If the $\text{H}\alpha$ line was measured with a signal to noise ratio of less than 2, or if it was measured in absorption, no extinction correction was applied. If the measured $\text{H}\beta$ flux failed these criteria, the extinction was calculated assuming an upper limit for the $\text{H}\beta$ flux of $2.3 \times 10^{-19} \text{ W m}^{-2}$ which is approximately the detection limit.

Finally, the $\text{H}\alpha$ fluxes were corrected for the $3''$ -diameter circular aperture of the fibres, considerably smaller than most of the galaxies in our sample. The correction was done by scaling the $\text{H}\alpha$ flux by the ratio of the total r -band flux to the r -band flux measured within the fibre itself. This procedure has been shown, by Hopkins et al. (2003), to provide excellent quantitative agreement with star-formation estimates from global galaxy properties such as radio, far-infrared and u -band continuum emission. This procedure assumes that the measured $\text{H}\alpha$ equivalent width is representative of the whole galaxy. For the volume-limited sample the median physical size probed by the $3''$ aperture is 4.4 kpc. The fibre therefore probes a significant fraction of the galaxy and this accounts for the reported accuracy in Hopkins et al. (2003).

2.3.2 Far-infrared continuum

Far infrared traces recent star formation, where the natal dust clouds still surround the young massive stars and re-processes most of their bolometric output. The effects of obscuration at these wavelengths are far less prominent than at optical/UV wavelengths, removing a potential source of systematic errors.

Flux densities at $60 \mu\text{m}$ and $100 \mu\text{m}$ were obtained for each galaxy in our volume limited catalogue by automated query of the SCANPI service¹, which co-adds individual *IRAS* scans at the position of each of the galaxies. The measurement in each band was rejected if the reported signal to noise was less than 2.5 or if the template correlation factor was less than 0.9. The FIR luminosity to SFR calibration we applied was the same as used by Hopkins et al. (2003), namely:

$$\psi_{\text{FIR}} (\text{M}_{\odot} \text{ yr}^{-1}) = \frac{f L_{\text{FIR}}}{1.39 \times 10^{36} \text{ W}}, \quad (2)$$

where

$$f = \begin{cases} 1 + \sqrt{\frac{2.186 \times 10^{35} \text{ W}}{L_{\text{FIR}}}} & L_{\text{FIR}} > 2.186 \times 10^{37} \\ 0.75 \left(1 + \sqrt{\frac{2.186 \times 10^{35} \text{ W}}{L_{\text{FIR}}}} \right) & L_{\text{FIR}} \leq 2.186 \times 10^{37}. \end{cases} \quad (3)$$

2.3.3 Specific Star Formation Rates

The star formation rates calculated above are not ideal for study of the triggering of star formation as they scale with galaxy mass. A more suitable measure is the specific star formation rate, defined as the SFR divided by the stellar mass. Approximate stellar masses were calculated from z -band ($\lambda_{\text{eff}} = 9097 \text{ \AA}$) luminosities, using $M_z(\odot) = 4.52$, as used by Yasuda et al. (2001), and assuming one solar luminosity corresponds to one solar mass. The Hubble parameter $H_0 = 70 \text{ km s}^{-1} \text{ Mpc}^{-1}$ is used throughout, for consistency with Hopkins et al. (2003).

To calculate the z -band luminosity, we used the reported Petrosian magnitudes as introduced by Petrosian (1976) and discussed

¹ Available at <http://irsa.ipac.caltech.edu/applications/Scanpi/>. Provided by NASA/IPAC Infrared Science Archive, which is operated by the Jet Propulsion Laboratory, California Institute of Technology, under contract with the National Aeronautics and Space Administration.

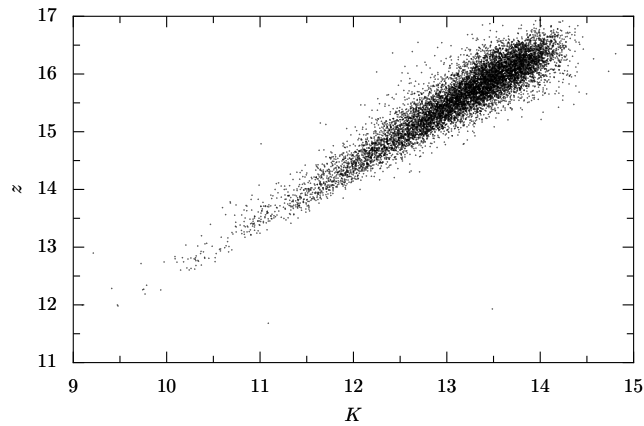


Figure 1. A scatter plot of K - vs. z -band magnitudes for the galaxies in the volume-limited sample detected in the 2MASS XSC.

extensively in the context of SDSS by Strauss et al. (2002). The fraction of galaxy light measured by Petrosian magnitudes depends only on the shape of the light profile of the galaxy and not on the surface brightness (Strauss et al. 2002). For this reason, if the effect of tidal interaction on near-infrared galaxy light distribution is to only change its characteristic length scale, there should be no bias in estimated masses of interacting and non-interacting systems.

The z -band light will inevitably suffer some intrinsic extinction. To assess whether it is an un-biased estimator of galaxy mass we have correlated our volume-limited sample with the Two Micron All Sky Survey (2MASS) Extended Source Catalogue (XSC) which is described in Jarrett et al. (2000). In Figure 1, we compare the Petrosian z -band magnitudes with total K -band magnitudes for the subset of galaxies which were detected in the XSC – there is a good correlation between them with a dispersion of 0.25 magnitudes in z . Since K -band magnitudes are generally believed to give an extinction independent estimate of galaxy mass we conclude that for this sample the z -band magnitude also provides an un-biased estimate. As a further check, we have investigated this correlation for close pairs ($r_p < 50$ kpc) and find it is unchanged from that shown in Figure 1.

2.4 Defining a Catalogue of Galaxy Pairs

To investigate the effects of galaxy interactions, we have identified the nearest companion galaxy to each member of our primary volume limited catalogue. The method used for this was influenced by the selection constraints of the spectroscopic follow up sample of the SDSS. In particular, the $55''$ minimum separation between targets on any one plate introduces a significant bias against finding close pairs of galaxies if only galaxies with measured spectra are considered. Therefore, we base our search for pairs on all the galaxies identified in the imaging data, using measured redshifts where available.

The procedure used was as follows: for each galaxy in the primary catalogue, a list of candidate companions out to a projected separation of 300 kpc was assembled from the SDSS imaging galaxy catalogues. Each of these candidates were then, in the order of increasing separation, evaluated according to following rules until a satisfactory match was found:

- If the angular separation between the primary galaxy and the candidate was less than three times the r -band Petrosian half-light radius of the primary (the mean of this value for the volume lim-

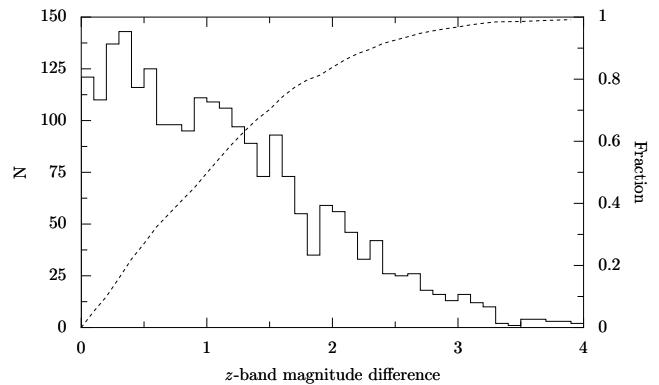


Figure 2. The distribution (solid line) and cumulative distribution (dashed line) of z -band magnitude differences in spectroscopically confirmed pairs.

ited sample is $9''$), the candidate was rejected. This is necessary to remove the small number of cases where the photometric pipeline incorrectly de-blends single galaxies into multiple components.

- If the candidate has a measured redshift, the recession velocity difference is evaluated: if it is less than 900 km s^{-1} the candidate is accepted, otherwise it is rejected. This is a relaxed constraint which, according to Patton et al. (2000, 2002), includes all potentially interacting systems and avoids a bias toward dynamically bound systems.

- If no redshift was measured, the z -band magnitude difference between the candidate and the primary galaxy is evaluated: if it is less than 2 magnitudes the candidate was accepted, otherwise it was rejected.

This procedure resulted in 12492 of the 13973 galaxies in the volume limited sample being identified with companions. Of these, 2038 have measured spectra, whilst the remaining systems have only imaging data.

2.4.1 Validity of Spectroscopic-Photometric Pairs

As described above, candidate pairs were not restricted to the MGS, but were taken from all the galaxies identified in the imaging survey. However, in the absence of redshift information, photometric properties must be used to determine if the pairing is just a projection effect or if the galaxies are physically close.

We adopted a relatively simple criterion, comparing the Petrosian z -band magnitudes of the two galaxies. This technique suffers both from incompleteness, when there is a large intrinsic luminosity difference between true companions, and contamination by background galaxies. As both of these effects depend sensitively on the cut-off brightness ratio, we now justify the choice of this quantity.

Our choice of $\Delta m_z = 2$ implies that companions which are fainter than the primary galaxy by more than about a factor of 6.3 in the z -band will be rejected, unless they have a measured redshift. The z -band was chosen for this comparison as it most closely traces the mass of the galaxy. To assess the significance of this incompleteness we have calculated the distribution of z -band magnitude differences in all pairs which have measured spectra, and therefore do not suffer from the above effect. The results, presented in Figure 2, show that $\Delta m_z = 2$ is in the tail of the distribution and that the completeness for this choice of Δm_z is approximately 80%.

We have also investigated the probability that a detected pair is due to background contamination as a function of the maximum

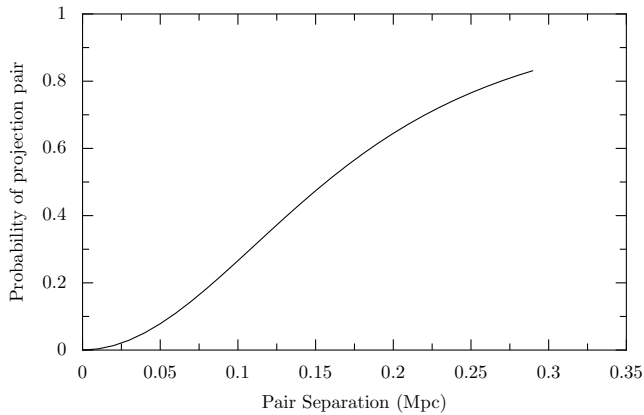


Figure 3. Mean probability of a non-physical pair as a function of separation from the primary galaxy.

magnitude difference. To do this we have used the galaxy count from Yasuda et al. (2001). The parameterised integrated counts, where m denotes the z -band magnitude, are

$$N(z\text{-mag} < m) = \frac{11.47}{\text{deg}^2} \times 10^{0.6(m-16)}. \quad (4)$$

The probability of a detected pair being due to contamination is then calculated as a function of physical separation and averaged over the whole of the primary catalogue. The results are presented in Figure 3. They show that at projected separation of over 150 kpc, contamination of our pair sample by background or foreground galaxies becomes a significant problem. Therefore, our results at separations greater than 150 kpc are significantly diluted by non-physical pairs; the reported separations in this regime can, however, be regarded as reliable lower limits of separation to the true nearest companion.

2.5 Concentration Index

Galaxy morphology has long been known to correlate strongly with the star-formation rate (e.g., Kennicutt 1998). Additionally, numerical simulations by Mihos & Hernquist (1996) show that the time dependence of gas inflow during interactions, and the star formation which results, depend sensitively on the structure of the progenitor galaxies, and in particular on the bulge to disk mass ratio. In order to measure accurately the effect of interactions on star formation, it is important to consider these effects.

The traditional classification of galaxy morphology is the Hubble sequence. There is a well established correlation between $H\alpha$ equivalent width and Hubble type, equivalent width increasing from zero (within observational errors) in E/S0 galaxies to 20–150 Å in late-type spiral and irregular galaxies, with the same trend shown between Sa through to Sc spirals (see Kennicutt & Kent 1983). The Hubble classification is based on three characteristics: the bulge-to-disk light ratio, tightness of spiral arms and degree of resolution of spiral arms. Besides being hard to automate, the Hubble classification is non-ideal for studies of star formation as the last of the three criteria in particular depends significantly on star formation. That is, the spiral arms are more likely to be resolved if there is significant star formation along them.

In this work we adopt an alternative morphological classification scheme, the concentration index, which is described in detail by Morgan (1958), Okamura et al. (1984), and Abraham et al.

(1994). The concentration index, C , is defined as the ratio of Petrosian 50%- to 90%-light radii as measured in the r -band. Low values of this quantity correspond to systems with high central concentrations of light which in turn are of an early morphological type. The correlation between classical morphological classification and the concentration index for a sample of galaxies taken from the SDSS is presented in Shimasaku et al. (2001).

We use the concentration index both to exclude early-type systems from our study of triggered star-formation and to examine the efficiency of this triggering as a function of morphological type. For the purpose of removing early-type systems, we exclude all galaxies with a concentration index less than 0.375, larger than the 0.33 value proposed by Shimasaku et al. (2001). In doing so, we reduce contamination of our late-type sample to less than 5% (see Figure 11 of Shimasaku et al. 2001), at the expense of completeness.

2.6 Pair Morphology

In the later stages of interaction it is often not possible to resolve the nuclei of interacting galaxies, especially in visible light, and even when they are resolved the automated algorithm in the SDSS photometric pipeline might not de-blend them. More importantly, the algorithm used to select nearest companions (Section 2.4) rejects all objects closer than three times the Petrosian half-light radius. As a result, our pair sample does not contain the closest pairs or merging objects. At the median redshift, and using the median half-light radius, the minimum galaxy separation corresponds to 14 kpc.

To assess the importance of this effect, we have visually inspected three sub-samples, each containing approximately 30 galaxies. The first consisted of the most actively star-forming objects, the second of medium star-forming objects and the third was a random control sample. In each case we evaluated the possibility that the galaxy is in the process of gravitational interaction via the presence of tidal arms and double nuclei. The results are presented in Section 3.3.

3 RESULTS

Our primary sample consists of 13973 galaxies of which 12492 have an identified companion. The distribution of morphological types, as determined by the concentration index (Section 2.5), of the galaxies in the primary sample, together with their companion, is shown in Table 1. The distribution of absolute star formation rates, ψ , and specific star formation rate, ψ_m , are shown in Figure 4. Here we distinguish between three morphologically-defined sub-samples: late-type ($C > 0.375$), early-type ($C \leq 0.33$) and mixed ($0.33 < C \leq 0.375$). As expected, given the good correlation between concentration index classification and Hubble type, the vast majority of star-forming systems are classified as late-type. The mean star formation rates are 0.7, 1.7, and 3.3 $M_\odot \text{ yr}^{-1}$ for the early, mixed and late type sub-samples respectively.

In this and following sections, we consider each pair to consist of a primary galaxy and companion and examine the star-formation rate of the primary galaxy in terms of the properties of the interacting pair.

3.1 Star formation as function of projected separation

To investigate the dependence of specific star formation rate, ψ_m , on true pair separation we consider firstly the dependence of ψ_m on projected separation, looking subsequently at the dependence

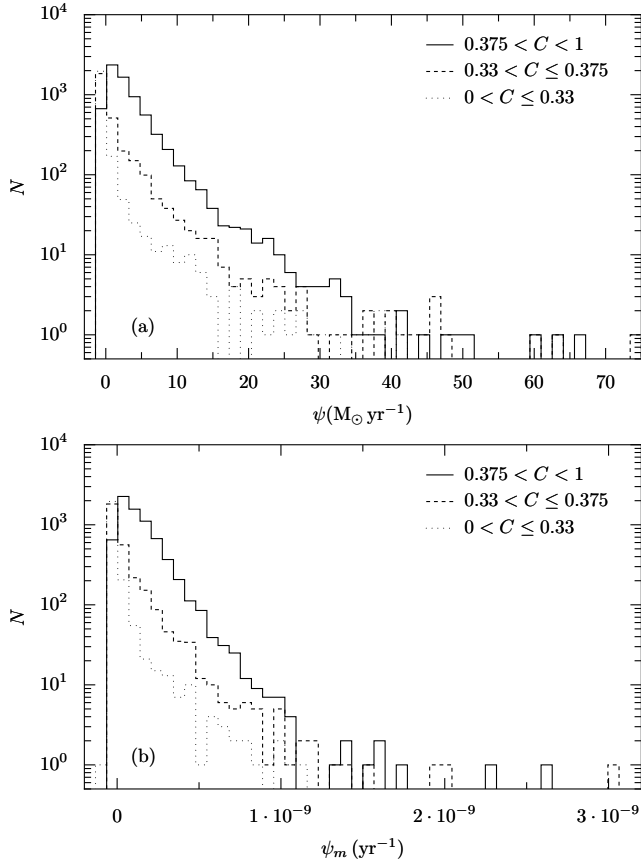
Table 1. Distribution across concentration index classes of galaxies in the volume limited sample and their companions.

Primary Galaxy	Total	Companion Galaxy			No companion ^a
		$C > 0.375$	$0.33 < C \leq 0.375$	$C \leq 0.33$	
$C > 0.375$	7936	5120	1500	555	761
$0.33 < C \leq 0.375$	3344	2064	681	270	329
$C \leq 0.33$	2693	1455	576	271	391
Total	13973	8639	2757	1096	1481

^a The number of galaxies with no companion identified within the 300 kpc maximum search radius.

Table 2. The dependence of the specific star formation rate on projected separation is characterised by fitting a two power-law function to the specific star formation rate vs pair separation data (Fig. 5) after its been divided according to morphological type.

Concentration Index bin	a_1 (10^{-11} yr^{-1})	β_1	a_2 (10^{-11} yr^{-1})	β_2
$0 < C \leq 0.33$	2.04	-0.53	0.11	1.19
$0.33 < C \leq 0.375$	6.30	-0.41	0.70	0.73
$0.375 < C \leq 1.0$	13.6	-0.04	2.90	-1.04

**Figure 4.** The distribution of (a) absolute and (b) specific star-formation rates for galaxies in the volume limited sample, split according to the concentration index into three subsamples.

on velocity separation. In Figure 5, we plot the mean specific star-formation rate against projected pair separation. The primary galaxy in each pair has been assigned, using the concentration index, to one of three morphological classes representing late-, mixed- and early-types (see Table 1). The data have been binned into bins 10 kpc wide for separations less than 100 kpc and bins 40 kpc wide for separations greater than 100 kpc. For each bin we have indicated the mean and the estimated statistical variance of the mean; the variance is dominated by sample variance rather than measurement errors. In each case we characterise the variation of ψ_m with pair separation, r_p , by fitting a simple two power-law function to the un-binned data:

$$\psi_m(r_p) = a_1 \left(\frac{r_p}{25 \text{ kpc}} \right)^{\beta_1} + a_2 \left(\frac{r_p}{25 \text{ kpc}} \right)^{\beta_2}. \quad (5)$$

The best-fitting parameters are detailed in Table 2.

For each morphological class, there is a significant increase in the specific star-formation rate at projected separations less than 30 kpc. For late-type systems there is some indication that the mean specific star-formation rate decreases systematically with projected separation out to separations of about 300 kpc where it reaches a value of $1.2 \times 10^{-10} \text{ yr}^{-1}$. Those systems classified as early- and mixed-types only show significant enhancement for projected separations less than about 25 kpc. The greater dispersion in these plots reflects the larger intrinsic range in the estimated star-formation rates in these systems, many of which are effectively zero.

The use of the concentration index as a morphological classifier does introduce some potential problems. Any enhancement in nuclear surface brightness of a galaxy will reduce the value of the concentration index for that system. In particular, an intense nuclear starburst may result in a late-type system being placed in the wrong morphological class. To examine this effect further we show in Figure 6 the mean concentration index for all systems as a function of projected separation. The concentration index peaks at a separation of around 75 kpc and rapidly declines at separations smaller than 50 kpc. Inspection by eye of the low concentration in-

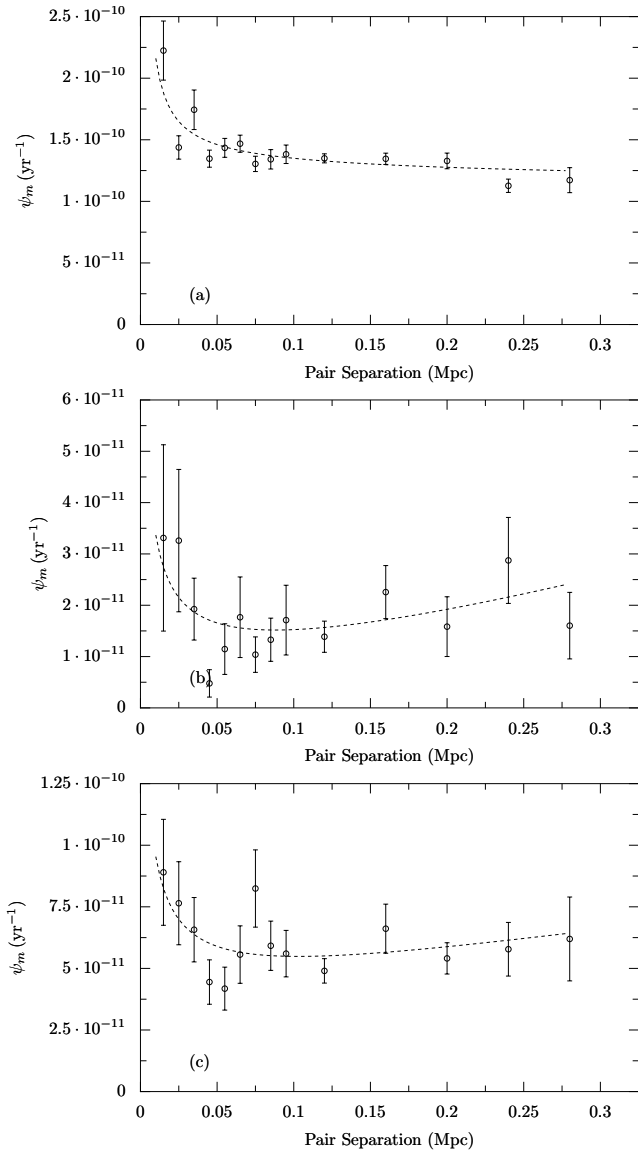


Figure 5. Specific star formation rates as a function of pair separation for late (a), early (b), and mixed (c) galaxy types.

dex systems at small separations, strongly suggest they are disk systems with pronounced nuclear starbursts. The enhancement in the specific star-formation rate at small physical separations for those systems which we have been classified as early- and mixed-type is likely, at least in part, to be explained by the misclassification of disc-galaxies with strong nuclear starbursts. We cannot eliminate the possibility that there is a real enhancement in star formation for intrinsic early-type systems for small physical separations to a companion; further study of this point requires an independent means of morphological classification.

Tidal distortion may also be contributing to the lowering of concentration index observed in Figure 6 for close pairs. A close encounter between two galaxies can lead to stripping of the more peripheral stellar material whilst leaving the central stellar distribution relatively undisturbed. The effect of such a distortion would be to increase the value of the Petrosian 90% light radius whilst leaving the Petrosian 50% light radius unchanged, reducing the concentration index. However, examination of the relative value of the 50

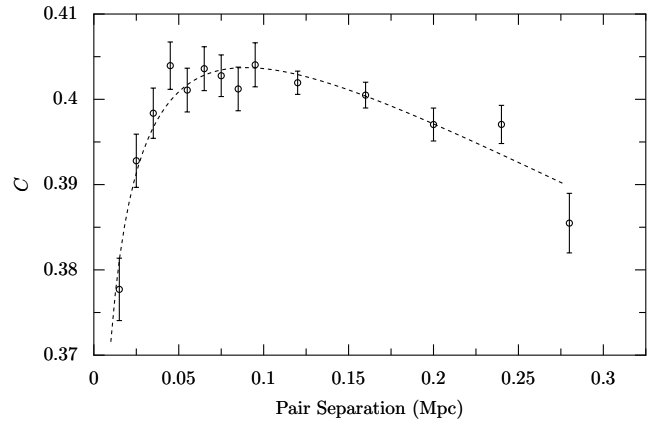


Figure 6. Mean concentration index, C , as a function of pair separation for the full volume limited sample. The dashed line is the least-squares best-fitting function of the form $C = a_1(r_p/25 \text{ kpc})^{\beta_1} + a_2(r_p/25 \text{ kpc})^{\beta_2}$; the best fit parameters are: $a_1 = 1.6$, $\beta_1 = 0.19$, $a_2 = -1.20$, and $\beta_2 = 0.24$.

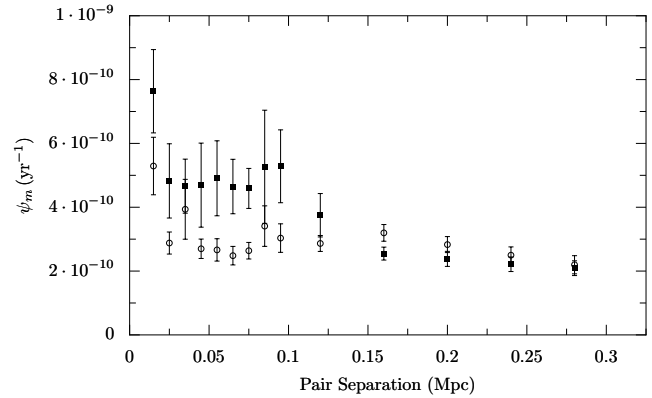


Figure 7. Far infrared (solid squares) and $H\alpha$ (open circles) estimated specific star formation rates as functions of pair separation for the sub sample detected by IRAS.

and 90% light radii with pair separation reveal both to decline for close pair separations, indicating that nuclear starbursts are likely to be the dominant factor in the reduction of concentration index at close pair separations.

The use of $H\alpha$ luminosity as the star-formation rate estimator involves corrections both for extinction and the finite size of the aperture as discussed in Section 2.3.1. These procedures may introduce subtle biases if, for example, the effect of tidal interaction is always to trigger a nuclear starburst. To investigate any such effects we compare results using the FIR and $H\alpha$ star-formation rate indicators – Figure 7. The comparison is limited to those systems for which both FIR and $H\alpha$ are available so this is inevitably biased towards systems with higher star formation rates. However, these are precisely the systems in which any problems associated with the use of $H\alpha$ as a star-formation rate estimator are likely to be the greatest. In fact, we find excellent agreement between the FIR and $H\alpha$ data both in terms of the trend with projected pair separation and the magnitude of the specific star formation rate. We conclude that the procedure used here to estimate star-formation rate from $H\alpha$ data gives an unbiased estimate of the true star-formation rate.

In order to further investigate the effect aperture correction has on our results, in Figure 8 we compare non-aperture corrected and aperture corrected star-formation rates as a function of separa-

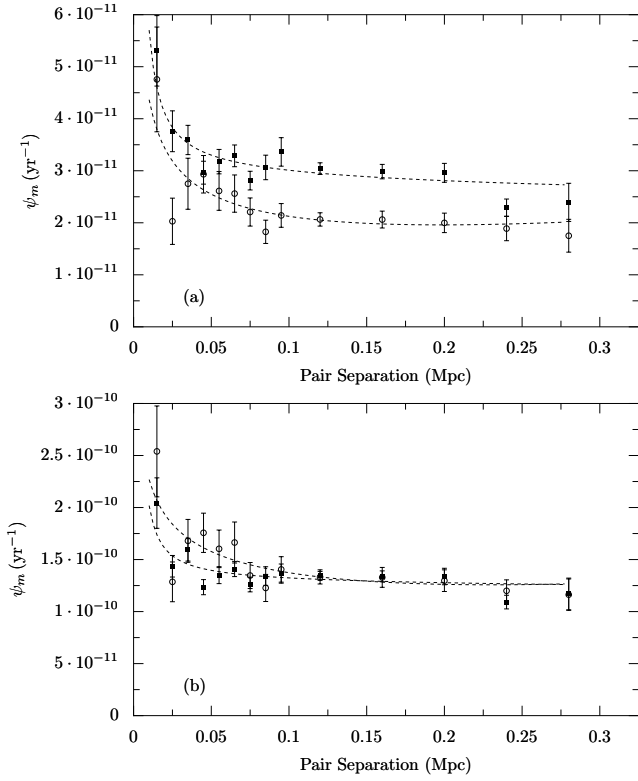


Figure 8. Comparison of (a) non-aperture corrected and (b) aperture-corrected star-formation rates versus separation for galaxies in two redshift bins: $0.04 < z \leq 0.07$ (open circles) and $0.07 < z \leq 0.1$ (full squares).

tion; the significance of the aperture correction is made clearer by splitting the sample into two redshift bins. It is quite clear that the non-aperture corrected data exhibit a similar trend to the corrected data, the main difference being a somewhat steeper rise of the SSFR at close separations. This is consistent with the majority of the triggered star formation occurring in the nuclear regions of the galaxies. Aperture correction brings the two sub-samples in surprisingly good agreement, though the higher corrected SSFR of the low-redshift subsample in the closest bin suggests that in the correction is over-estimated in systems with strong nuclear star formation.

In Figure 9, we show the distribution of specific star-formation rates for two sub-samples of late type galaxies: one of galaxies with companion within 50 kpc projected separation, and the other with companions at projected separation greater than 200 kpc or no companion at all. The Kolmogorov-Smirnov (K-S) test indicates, at a significance level greater than 99.9%, that the star-formation rates in these two sub-samples are drawn from different parent distributions. The distributions only differ significantly for specific star-formation rates above approximately $3 \times 10^{-10} \text{ yr}^{-1}$ suggesting that the observed increase in the mean specific star-formation rate for systems with close companions is dominated by systems showing significant increases in their rate of star formation. To investigate this further, we show in Figure 10 and Table 3 the variation in ψ_m with projected separation for late-type systems binned according to the absolute star-formation rate: low star-forming ($0 < \psi < 3M_{\odot} \text{ yr}^{-1}$), medium star-forming ($3M_{\odot} \text{ yr}^{-1} < \psi < 10M_{\odot} \text{ yr}^{-1}$), and highly star-forming ($10M_{\odot} \text{ yr}^{-1} < \psi$). The late-type systems in the lowest star formation rate bin $0 < \psi < 3M_{\odot} \text{ yr}^{-1}$ show no enhancement of specific star-formation rate with decreasing pair

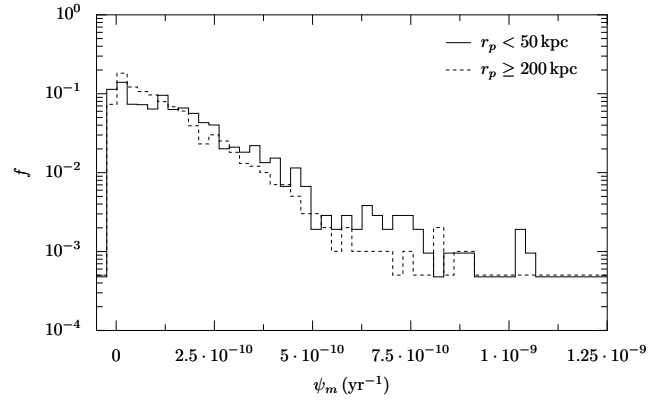


Figure 9. The relative distribution of specific star-formation rates for galaxies from the late-type volume limited sample with close companions (solid line) and no companions or companions which are separated by more than 200 kpc (dashed line).

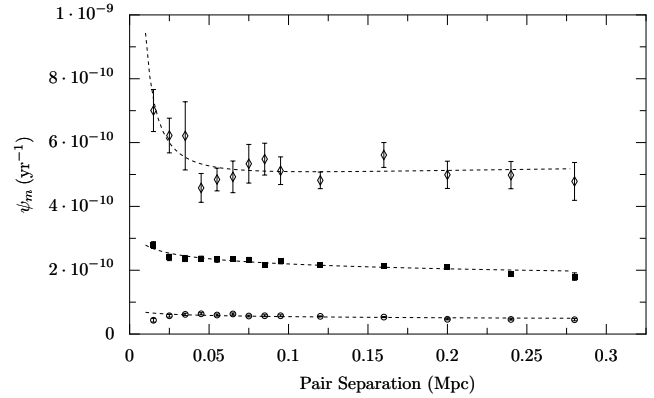


Figure 10. Specific star formation versus separation for three sub-samples selected according to absolute star formation rate: $0 < \psi < 3M_{\odot} \text{ yr}^{-1}$, $3M_{\odot} \text{ yr}^{-1} < \psi < 10M_{\odot} \text{ yr}^{-1}$ and $\psi > 10M_{\odot} \text{ yr}^{-1}$.

separation. In contrast both of the higher star-formation rate bins ($3M_{\odot} \text{ yr}^{-1} < \psi < 10M_{\odot} \text{ yr}^{-1}$ and $\psi > 10M_{\odot} \text{ yr}^{-1}$) show a clear increase in specific star-formation rate with decreasing projected separation. As is clear from the plots, and the best-fitting parameters given in Table 3, this enhancement is most significant at the highest star-formation rates.

In summary, we find strong evidence for an enhancement in the specific star-formation rate in late-type systems as a function of projected separation to the nearest companion. Within a projected separation of 50 kpc there is a very significant increase in ψ_m and this can be attributed to the contribution from systems showing the largest star-formation rates.

3.2 Star formation properties as a function of recession velocity separation

In approximately one-fifth of our volume limited sample the companion galaxy has a measured SDSS spectrum, and therefore, in most cases, a measured redshift. In Figure 11 we examine the effect of the recession velocity difference on star formation rate for these galaxies. The best-fitting parameters from fitting a two power-law model are shown in Table 4. The data reveal a decline in the specific star-formation rate with increasing recession velocity.

Table 3. Parameters obtained when fitting a two power-law function to plots of specific star formation rate as a function of pair separation for three sub-samples of systems, selected according to SFR.

SFR range ($M_{\odot} \text{ yr}^{-1}$)	a_1 (yr^{-1})	β_1	a_2 (yr^{-1})	β_2
$0 < \psi \leq 3$	3.26×10^{-11}	-0.10	2.98×10^{-11}	-0.09
$3 < \psi \leq 10$	1.40×10^{-10}	-0.10	1.14×10^{-10}	-0.10
$10 < \psi \leq 1000$	1.43×10^{-10}	-1.37	4.03×10^{-10}	0.05

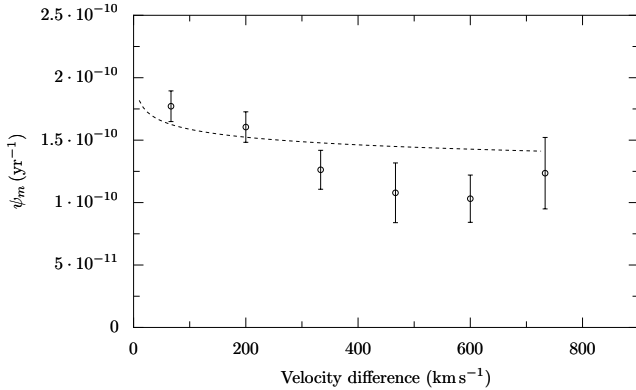


Figure 11. Specific star-formation rate of late type galaxies ($C > 0.375$) as a function of velocity separation.

Table 4. Parameters obtained when fitting a two power-law function to the plot of specific star formation rate as a function of the recessional velocity of spectroscopic galaxy pairs.

a_1 (yr^{-1})	β_1	a_2 (yr^{-1})	β_2
4.56×10^{-10}	0.05	1.43×10^{-10}	-1.38

city difference out to 900 km s^{-1} . The magnitude of this effect is smaller than that observed between specific star-formation rate and projected separation. The steepest decline is seen at small velocity differences.

A correlation between projected separation and velocity difference may be expected if, for example, all systems were bound. We find no correlation between these two quantities for this sample; the mean velocity separation is $\sim 200 \text{ km s}^{-1}$ and is independent of projected separation.

3.3 Optical Morphology

Optical and near-infrared imaging of *IRAS* selected galaxies has revealed that the fraction of objects which are interacting/merging increases systematically with increasing infrared luminosity. For example, Sanders & Mirabel (1996) find this fraction increases from about 10% at $\log(L_{\text{FIR}}/L_{\odot}) = 10.5\text{--}11$ to essentially 100% at $\log(L_{\text{FIR}}/L_{\odot}) > 12$.

As discussed in Section 2.4, our procedure for finding companions misses very close companions and actively merging systems. The results of the previous two sections are subject to this bias. In particular, systems which are undergoing strong enhancements in their star-formation rate due to ongoing mergers are likely

to appear in our catalogue over the full range of projected separations (and/or recessional velocity difference). Such systems will therefore only contribute to masking any real effect due to tidal interactions.

We have therefore examined by eye the morphologies of 81 galaxies in our sample. The 81 galaxies examined were selected in three ways:

A: The twenty-four most highly star forming galaxies; equivalent infrared luminosities $\log(L_{\text{FIR}}/L_{\odot}) > 11.42$.

B: Twenty-five galaxies with moderately active star formation; equivalent infrared luminosities in the range $11.10 < \log(L_{\text{FIR}}/L_{\odot}) < 11.13$.

C: A random control sample of thirty-two galaxies.

Among the 24 galaxies in group A, 38% show evidence of being merging systems. This fraction drops to 20% in group B and 6% in the control sample. The trend observed in the *IRAS*-selected samples of increasing optical disturbance with increasing infrared luminosity is therefore reflected in our volume-limited sample. The large fraction of merger systems at the high star-formation rates can only reduce the observed anti-correlation between star formation and projected separation. We discuss these effects further in Section 4.

3.4 Dependence on the properties of the interaction

We do not expect all tidal interactions to lead to enhanced star formation. How effective a given interaction is at triggering gas inflow etc. may depend not only on the properties of the perturbed galaxy (which we have examined in the previous section), but also upon the nature of the perturber. The nature of the perturbing galaxy can be probed in two ways: its morphological class and mass.

In Figure 12 we show the distribution of specific star-formation rates for late-type galaxies with a companion within 50 kpc. We split the pairs into three sub-samples depending on the morphological type of the perturber: late-late, late-mixed and late-early pairs. There are no significant differences between these sub-samples: the Kolmogorov-Smirnov (K-S) test applied between the late-late and late-early distributions gives a formal significance of only 20% that they are drawn from different distributions.

We investigate the effect of companion mass in Figure 13. Again, we split those systems which have companions with projected separations less than 50 kpc into three sub-samples according to the z -band magnitude difference between the primary and companion galaxy [$\Delta m_z = m_z(\text{primary}) - m_z(\text{companion})$]. For all specific star-formation rates we find an excess of systems where the companion is of lower mass than the primary galaxy. This effect is mainly due to form of the luminosity function which rises steeply to lower luminosities at the limit of our primary sample. Therefore, for real physical pairs, a galaxy of a given luminosity is more

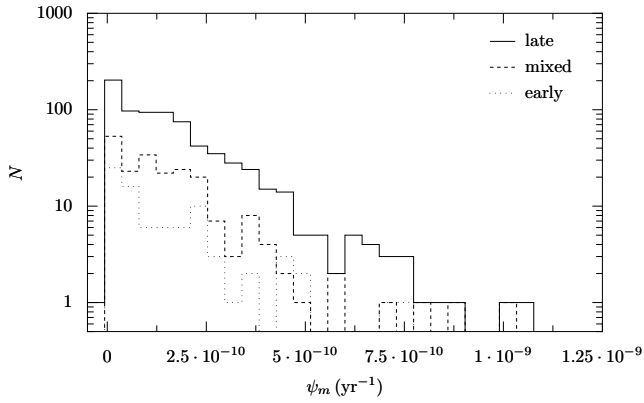


Figure 12. Distribution of specific star formation rates for galaxies with companions closer than 50 kpc, split according to the morphological type of the companion.

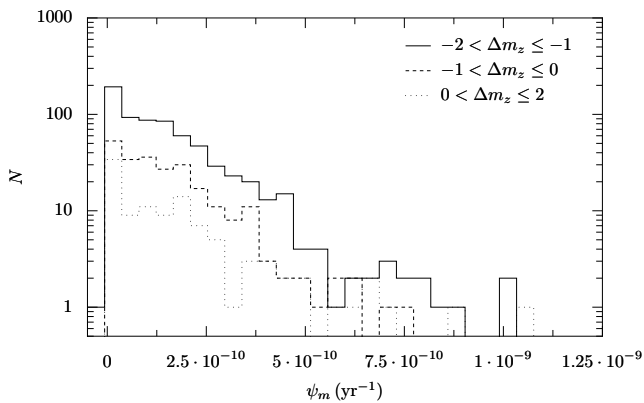


Figure 13. Distribution of specific star formation rates for galaxies with pairs closer than 50 kpc, split according to z -band magnitude difference.

likely to be interacting with a galaxy of lower luminosity. We have used the K-S test to compare the SSFR of the three subsamples. We tested the null hypothesis that the three distributions are all drawn from the same parent distribution. We find no evidence to reject the null hypothesis – the formal confidence level that the distributions are drawn from different populations is 50%.

4 DISCUSSION

The high-quality data from the SDSS has enabled us to construct a sample of galaxies with companions which is an order of magnitude larger than those used in previous studies. Such a data set enables us to investigate not only the effect of tidal interactions on star formation within galaxies, but also to examine this as a function of morphological type and nature of the perturbing galaxy. Interpretation of our results is made easier by using a substantially complete volume- and luminosity-limited sample.

We begin our discussion by briefly reviewing sources of possible error and bias in our sample. To estimate star-formation rate we have used the $H\alpha$ luminosity from the SDSS. This was corrected for extinction using measured $H\beta$ data and then corrected for the finite aperture size (see Section 2.3.1). By constraining the lower redshift limit of the sample to 0.03 the aperture correction is minimised. As shown in Hopkins et al. (2003) this procedure leads to measurements of the star-formation rate in agreement with

other estimators, however, a residual effect remains. For systems in which star formation is dominated by a nuclear starburst which falls within the SDSS fibre, the aperture correction will tend to overestimate the star-formation rate to some extent. On the other hand, if the majority of star formation is off-nuclear, or if the fibre is not accurately positioned on the nucleus, then the aperture correction will not recover the true star-formation rate. Undoubtedly, these effects occur in measurements of individual objects, however the data shown in Figure 8 suggest that on the whole the aperture correction is a useful way of estimating the global star-formation rates.

We have also made use of *IRAS* FIR data to give an independent estimate of star-formation rate for those objects in the volume limited sample that are detected. These systems are the most actively star-forming systems in the sample, and therefore most likely to suffer significant problems due to the aperture correction and extinction. We have found that the results based on $H\alpha$ and FIR are in good agreement suggesting that the $H\alpha$ -based estimate of the star-formation rate is sufficiently unbiased for the purposes of this study. We do find, however, that in systems with close pairs, the $H\alpha$ estimated SFR are approximately 30% smaller than those estimated using the FIR data – an indication perhaps that we underestimate the extinction in these systems.

Although we have removed all systems which show any spectroscopic evidence of having an AGN, it is possible that highly obscured AGN are present in our sample. However, given our procedure, it seems likely that if such systems are present their $H\alpha$ fluxes will be dominated by star formation. On the other hand, their FIR fluxes – which more closely measure bolometric output – may be enhanced by the AGN; but, this can only make the correlation between the $H\alpha$ and FIR measured star-formation rates worse.

As discussed in Section 2.4, closest companions were selected on the basis of z -band magnitude difference in the projected separation range $3 \times$ Petrosian half-light radius $< r_p < 300$ kpc, and using spectroscopic data in the 20% of cases where it was available. This approach has the advantage that our sample is complete to a minimum pair separation of about 15 kpc and to a well defined z -band luminosity difference. This completeness comes at the cost of contamination by projection effect pairs; we have shown that these only become significant at separations greater than 150 kpc. In these cases the distance to the closest companion represents a lower-limit to the true separation. Since this contamination is only significant at larger separations it should not affect the interpretation of our results.

The imposed minimum pair separation and intrinsic difficulty in de-blending galaxies with overlapping disks does mean we will inevitably miss very close pairs and merging systems. We note that of the 9 systems in the highest SFR bin (Section 3.3) that are classified as actively merging, all but one have been erroneously paired with distant galaxies.

We observe an enhancement in the specific star-formation rate in late-type systems with a close companion ($r_p \lesssim 50$ kpc). This result is similar to that found by Barton et al. (2000) and Lambas et al. (2003). A quantitative comparison to the results of Lambas et al. (2003) is possible. The functional form used to fit the data in Lambas et al. (2003) is a single power-law of the form $\langle b \rangle = a_1 r_p^\beta$ where b is the *birth parameter* which should be proportional to ψ_m . We have fitted our data using a similar functional form, restricting the range of projected separations to that used by Lambas et al. (2003) [$0 < r_p < 100 \times (0.7)^{-1}$ kpc]. After converting results to a common distance scale we find that we obtain agreement with Lambas et al. (2003) only if we apply the additional constraint

$\psi_m > 2 \times 10^{-11} \text{ yr}^{-1}$, which accounts for a bias towards more star forming systems in Lambas et al. (2003).

The larger sample size, and additional parameters available in the SDSS have enabled us to examine these basic results in greater detail.

Although the strongest enhancement in the specific star-formation rate occurs for small physical projected separations, we also find that for late-type galaxies, there appears to be a systematic decrease of specific star formation with increasing companion separation out to 300 kpc. A similar trend may also be present in the data of Lambas et al. (2003) (see their Figure 1) although Lambas et al. do not reach this conclusion. This long-range correlation between star formation and pair separation is seen only in late-type systems, i.e., those with concentration indices > 0.375 .

It should be noted that the combination of significant projection pair contamination at large separations and the morphological separation into only three bins might contrive to make galaxies of slightly earlier morphological type biased towards pairs at large separations which could produce a correlation similar to that which is observed.

An interpretation of this effect as due to triggering of star-formation would, however, be consistent with the predictions of Mihos & Hernquist (1996), who show that galaxies with weak bulge components are more susceptible to formation of bars during interaction. The presence of the bar provides the mechanism for gas flow towards the nucleus, leading to enhanced star formation over a prolonged period of time, even when the galaxies are still widely separated. Such weak-bulge systems constitute the highest concentration index systems in our sample. In contrast, systems with strong bulges (i.e., lower concentration indices) are stabilised against bar formation by the presence of the bulge. As a result, the onset of star formation is delayed until the final stages of merger.

It is clear from our data that, if only actively star-forming systems are considered (e.g., $\psi > 10 M_\odot \text{ yr}^{-1}$, Figure 10), the increase of the average star formation at close separations is much higher. This suggests that the significance of interactions will be somewhat overestimated in studies which are biased towards selecting star-forming systems. Our data for the FIR detected sub-sample demonstrate this quite clearly.

We also find a surprisingly tight relationship between the concentration index and pair separation. The steep decline of the concentration index at projected separations below 50 kpc is most easily explained if there exists a population of systems with nuclear starbursts at these separations. If this is the case, it is quite likely that a few systems with strong disk components and intense star formation have been misclassified, using the concentration index, as intermediate types. It is possible such systems are responsible for some, or even most, of the enhancement of SFR in galaxies of intermediate type with close pairs.

The specific star-formation rate is found to decrease with increasing recessional velocity separation out to the largest velocity separations, suggesting that fly-by encounters, in which the two systems are not on bound orbits, do contribute to enhanced star formation. The specific star-formation rate appears to be a weaker function of velocity difference than of projected physical separation, however this may be a result of dilution of the velocity results due to line of sight projection effects. Comparing our results with those of Lambas et al. (2003) we note a similar percentage drop in the SSFR over the velocity range 0–200 km s⁻¹, however, we do not observe the marked change in gradient at $\sim 350 \text{ km s}^{-1}$ they observe.

The nature of the perturber does not appear significant in de-

termining star formation enhancement. We find no difference in the effectiveness of triggering star formation between late-type / late-type and late-type / early-type interactions. Further, we find no evidence for a dependence of the specific star-formation rate on the mass of the companion. This is in contrast both to the results of Donzelli & Pastoriza (1997) and Lambas et al. (2003). Donzelli & Pastoriza (1997) examine star formation enhancement in a sample of 27 physical pairs consisting of a main galaxy and a companion that has approximately half the diameter. They find that the star formation enhancement is much stronger ($\sim 50\%$ on average) in the minor components of the pairs. In contrast, Lambas et al. (2003), dividing their pair sample into minor and major merger candidates according to the relative luminosity of the component galaxies, find that the bright components of minor merger pairs show a higher probability of having enhanced star formation. Comparing the star formation enhancement in major mergers, they find no significant difference between the two components. Our results may be reconciled with those of Lambas et al. (2003); as is clear from Figure 13 the mean of the distribution for the sub-sample with $-2 < \Delta m_z < -1$ is greater than that for $0 < \Delta m_z < 2$, however this is caused by small number statistics at high specific star formation rates.

An interpretation which is consistent with our own results and those of Lambas et al. (2003) is as follows. The probability of a galaxy undergoing enhanced star formation depends strongly on the properties of the galaxy itself (availability of gas etc.) and on the nature of the orbital interaction with its companion. However the mass of the companion is of less importance – we only probe mass ratios less than a factor of ~ 6 , we would expect very much larger mass ratios to show a different effect. There is a strong tendency for a given system to be involved in an interaction with a lower-mass companion (a “minor” interaction), but we believe this results simply from the form of the luminosity function. These results are still in conflict with the findings of Donzelli & Pastoriza (1997) – in this case it is not clear how their sample selection and small number statistics would effect their conclusions.

In this work, we have not explicitly considered the effect of environment on galaxy star-formation rates. Our volume-limited sample is selected from the MGS which only contains galaxies with spectroscopic data, and therefore is biased slightly *against* galaxies in dense environments, where fibre collisions are more likely. Our pair finding procedure however uses all the data, and therefore does not suffer from this bias. Thus, although high-density regions may be somewhat under-represented in our primary sample, the pair separations should be unbiased.

As noted in the introduction, a number of studies have examined the relationship between star-formation rates and the environment (e.g., Gómez et al. 2003; Lewis et al. 2002; Hashimoto et al. 1998) – these studies all find a reduction in the mean star-formation rate in dense environments. However, interpreting these results is difficult because of the well-known and very strong correlation between morphological type and environment (e.g., Dressler 1980; Goto et al. 2003), and the correlation of morphological type and star formation (e.g., Kennicutt 1998). Other galaxy properties are also known to correlate with environment: galaxies are, for example, on average more luminous in rich clusters ($M_{bJ}^* = -20.07 \pm 0.07$, De Propris et al. 2003) and marginally more luminous in groups ($M_{bJ}^* = -19.90 \pm 0.03$, Martínez et al. 2002) as compared to the field ($M_{bJ}^* = -19.79 \pm 0.04$, Madgwick et al. 2002).

Our results show enhanced specific star-formation rates at close pair separations. The simplest interpretation, which we favour, is that this is indicative of tidally-triggered star formation.

Indeed, tidally triggered conversion of gas into stars during cluster assembly has been suggested as the *cause* of the relation between density of environment and star formation (Balogh et al. 2004, and reference therein). Alternatively, it could be a result of some other process, also responsible for the observed correlation between galaxy properties and environment. This however seems unlikely for the following reasons. If close pairs are more likely in dense environments, the works cited above suggest that their star-formation rate would, on average, be reduced and their luminosity increased thereby further reducing their specific star-formation rate. We, however, observe the opposite effect. Our observations could be explained by environmental effects if close pairs are in fact more likely in the field where the average star-formation rate is higher. A full analysis of these effects is beyond the scope of the present paper, but will be the subject of a forthcoming investigation.

5 CONCLUSIONS

We have used SDSS DR1 imaging and DR2 spectroscopy products to construct a catalogue of nearest companions for a volume and luminosity limited sample of galaxies drawn from the Main Galaxy Sample. Star formation rates for the volume-limited sample have been calculated from extinction and aperture corrected $H\alpha$ luminosities, and *IRAS* data where available. We used *r*-band concentration indices as a proxy to morphological classification and *z*-band luminosities to estimate galaxy masses. Our results indicate that:

(i) Mean star formation rates in late-type systems show clear correlation with distance to the nearest companion. This correlation extends out to projected separations of 300 kpc.

(ii) We show this correlation is more pronounced in actively star-forming systems.

(iii) The decrease of star formation rate with increasing separation is less sudden for systems with a high concentration index (i.e., small bulge components) supporting theoretical predictions that they are more susceptible to long-range triggering.

(iv) We observe a decline in the mean star-formation rate with increasing recession velocity difference for those galaxy pairs where a redshift has been measured for both galaxies. The magnitude of this effect is small when compared with projected separation.

(v) We observe a tight relationship between the concentration index and pair separation which peaks at $r_p = 75$ kpc and declines rapidly at smaller separations. We interpret this trend as due to the presence of tidally-triggered nuclear starbursts in systems with small projected separation.

REFERENCES

- Abraham R. G., Valdes F., Yee H. K. C., van den Bergh S., 1994, *ApJ*, 432, 75
- Arp H., 1966, *Atlas of peculiar galaxies*. Pasadena: California Inst. Technology, 1966
- Balogh M., Eke V., Miller C., Lewis I., Bower R., Couch W., Nichol R., Bland-Hawthorn J., Baldry I. K., Baugh C., Bridges T., Cannon R., Cole S., Colless M., Collins C., Cross N., Dalton G., de Propris R., Driver S. P., Efstathiou G., Ellis R. S., Frenk C. S., Glazebrook K., Gomez P., Gray A., Hawkins E., Jackson C., Lahav O., Lumsden S., Maddox S., Madgwick D., Norberg P., Peacock J. A., Percival W., Peterson B. A., Sutherland W., Taylor K., 2004, *MNRAS*, 348, 1355
- Barton E. J., Geller M. J., Kenyon S. J., 2000, *ApJ*, 530, 660
- Bergvall N., Laurikainen E., Aalto S., 2003, *A&A*, 405, 31
- Bushouse H. A., Werner M. W., Lamb S. A., 1988, *ApJ*, 335, 74
- Cardelli J. A., Clayton G. C., Mathis J. S., 1989, *ApJ*, 345, 245
- Cole S., Lacey C. G., Baugh C. M., Frenk C. S., 2000, *MNRAS*, 319, 168
- De Propris R., Colless M., Driver S. P., Couch W., Peacock J. A., Baldry I. K., Baugh C. M., Bland-Hawthorn J., Bridges T., Cannon R., Cole S., Collins C., Cross N., Dalton G. B., Efstathiou G., Ellis R. S., Frenk C. S., Glazebrook K., Hawkins E., Jackson C., Lahav O., Lewis I., Lumsden S., Maddox S., Madgwick D. S., Norberg P., Percival W., Peterson B., Sutherland W., Taylor K., 2003, *MNRAS*, 342, 725
- Donzelli C. J., Pastoriza M. G., 1997, *ApJS*, 111, 181
- Dressler A., 1980, *ApJ*, 236, 351
- Fukugita M., Ichikawa T., Gunn J. E., Doi M., Shimasaku K., Schneider D. P., 1996, *AJ*, 111, 1748
- Gómez P. L., Nichol R. C., Miller C. J., et al., 2003, *ApJ*, 584, 210
- Goto T., Yamauchi C., Fujita Y., Okamura S., Sekiguchi M., Smail I., Bernardi M., Gomez P. L., 2003, *MNRAS*, 346, 601
- Hashimoto Y., Oemler A. J., Lin H., Tucker D. L., 1998, *ApJ*, 499, 589
- Hopkins A. M., Miller C. J., Nichol R. C., Connolly A. J., Bernardi M., Gómez P. L., Goto T., Tremonti C. A., Brinkmann J., Ivezić Ž., Lamb D. Q., 2003, *ApJ*, 599, 971
- Jarrett T. H., Chester T., Cutri R., Schneider S., Skrutskie M., Huchra J. P., 2000, *AJ*, 119, 2498
- Kennicutt R. C., 1998, *ARA&A*, 36, 189
- Kennicutt R. C., Kent S. M., 1983, *AJ*, 88, 1094
- Kennicutt R. C., Roettiger K. A., Keel W. C., van der Hulst J. M., Hummel E., 1987, *AJ*, 93, 1011
- Lambas D. G., Tissera P. B., Alonso M. S., Coldwell G., 2003, *MNRAS*, 346, 1189
- Larson R. B., Tinsley B. M., 1978, *ApJ*, 219, 46
- Lewis I., Balogh M., De Propris, et al., 2002, *MNRAS*, 334, 673
- Madgwick D. S., Lahav O., Baldry I. K., Baugh C. M., Bland-Hawthorn J., Bridges T., Cannon R., Cole S., Colless M., Collins C., Couch W., Dalton G., De Propris R., Driver S. P., Efstathiou G., Ellis R. S., Frenk C. S., Glazebrook K., Jackson C., Lewis I., Lumsden S., Maddox S., Norberg P., Peacock J. A., Peterson B. A., Sutherland W., Taylor K., 2002, *MNRAS*, 333, 133
- Martínez H. J., Zandivarez A., Merchán M. E., Domínguez M. J. L., 2002, *MNRAS*, 337, 1441
- Mihos J. C., Hernquist L., 1996, *ApJ*, 464, 641
- Morgan W. W., 1958, *PASP*, 70, 364
- Okamura S., Kodaira K., Watanabe M., 1984, *ApJ*, 280, 7
- Patton D. R., Carlberg R. G., Marzke R. O., Pritchet C. J., et al., 2000, *ApJ*, 536, 153
- Patton D. R., Pritchet C. J., Carlberg R. G., Marzke R. O., et al., 2002, *ApJ*, 565, 208
- Petrosian V., 1976, *ApJ*, 209, L1
- Salpeter E. E., 1955, *ApJ*, 121, 161
- Sanders D. B., Mirabel I. F., 1996, *ARA&A*, 34, 749
- Shimasaku K., Fukugita M., Doi M., Hamabe M., et al., 2001, *AJ*, 122, 1238
- Stoughton C., Lupton R. H., Bernardi M., Blanton M. R., et al., 2002, *AJ*, 123, 485
- Strauss M. A., Weinberg D. H., Lupton R. H., Narayanan V. K., et al., 2002, *AJ*, 124, 1810
- Toomre A., Toomre J., 1972, *ApJ*, 178, 623
- Veilleux S., Osterbrock D. E., 1987, *ApJS*, 63, 295
- Whitmore B. C., Gilmore D. M., Jones C., 1993, *ApJ*, 407, 489

Yasuda N., Fukugita M., Narayanan V. K., Lupton R. H., et al.,
2001, *AJ*, 122, 1104
York D. G., Adelman J., Anderson J. E., Anderson S. F., et al.,
2000, *AJ*, 120, 1579

ACKNOWLEDGEMENTS

Funding for the creation and distribution of the SDSS Archive has been provided by the Alfred P. Sloan Foundation, the Participating Institutions, the National Aeronautics and Space Administration, the National Science Foundation, the U.S. Department of Energy, the Japanese Monbukagakusho, and the Max Planck Society. The SDSS Web site is <http://www.sdss.org/>.

The SDSS is managed by the Astrophysical Research Consortium (ARC) for the Participating Institutions. The Participating Institutions are The University of Chicago, Fermilab, the Institute for Advanced Study, the Japan Participation Group, The Johns Hopkins University, Los Alamos National Laboratory, the Max-Planck-Institute for Astronomy (MPIA), the Max-Planck-Institute for Astrophysics (MPA), New Mexico State University, University of Pittsburgh, Princeton University, the United States Naval Observatory, and the University of Washington.

This research has made use of the NASA/IPAC Extragalactic Database (NED) which is operated by the Jet Propulsion Laboratory, California Institute of Technology, under contract with the National Aeronautics and Space Administration.

This research has made use of NASA's Astrophysics Data System.

This research has made use of the NASA/ IPAC Infrared Science Archive, which is operated by the Jet Propulsion Laboratory, California Institute of Technology, under contract with the National Aeronautics and Space Administration.

This publication makes use of data products from the Two Micron All Sky Survey, which is a joint project of the University of Massachusetts and the Infrared Processing and Analysis Center/California Institute of Technology, funded by the National Aeronautics and Space Administration and the National Science Foundation.

We would like to thank Sebastian Jester for answering numerous queries about the SDSS. Finally, we thank the referee for detailed and helpful comments on the first version of the paper.